Unsteady Transonic Flow Calculations for Two-Dimensional Canard-Wing Configurations

John T. Batina*
NASA Langley Research Center, Hampton, Virginia

Unsteady transonic flow calculations for aerodynamically interfering airfoil configurations are performed as a first step toward solving the three-dimensional canard-wing interaction problem. These calculations are performed by extending the XTRAN2L two-dimensional unsteady transonic small-disturbance code to include an additional airfoil. Unsteady transonic forces due to plunge and pitch motions of a two-dimensional canard and wing are presented. Results for a variety of canard-wing separation distances reveal the effects of aerodynamic interference on unsteady transonic airloads. Aeroelastic analyses employing these unsteady airloads demonstrate the effects of aerodynamic interference on aeroelastic stability and flutter. For the configurations studied, increases in wing flutter speed result with the inclusion of the aerodynamically interfering canard.

Nomenclature

a = nondimensional elastic axis location, positive aft of midchord
b = wing semichord
c = wing chord
c_{ℓ_c} = canard lift coefficient
c_{ℓ_w} = wing lift coefficient
C_p = steady pressure coefficient
C_p^* = critical pressure coefficient for sonic flow
D = canard-wing vertical separation distance in units of wing chord (see Fig. 1a)
h = plunge displacement in units of wing chord
h_1 = plunge pulse amplitude
k = reduced frequency, $=\omega b/U$
m = mass of wing per unit span
M = freestream Mach number
$\bar{q}$ = nondimensional flight dynamic pressure, $=(U/(b\omega_\alpha\sqrt{\mu}))^2$
$\bar{q}_F$ = nondimensional flutter dynamic pressure, $=(U_F/(b\omega_\alpha\sqrt{\mu}))^2$
Q_{ij} = unsteady aerodynamic coefficient, ith generalized force due to jth mode of motion (see Table 1)
r_α = radius of gyration of wing about elastic axis
s = Laplace transform variable, $=\sigma+i\omega$
S = canard-wing horizontal separation distance in units of wing chord (see Fig. 1a)
t = time
U = freestream velocity
U_F = flutter speed
V_F = flutter speed index, $=U_F/(b\omega_\alpha\sqrt{\mu})$
x = distance from leading edge positive downstream along canard or wing
x_α = distance from elastic axis to mass center nondimensionalized by b
$\{Z\}$ = state vector
α = angle of attack of canard or wing
α_w = wing pitch angle
α_0 = mean angle of attack of canard or wing
α_1 = pitch pulse amplitude
ΔC_p = lifting pressure coefficient
ΔM = Mach number contour interval
μ = wing mass ratio, $=m/\pi\rho b^2$
ρ = freestream air density
τ = nondimensional time, $=Ut/b$
ω = angular frequency
ω_h, ω_α = wing uncoupled plunge and pitch natural frequencies, respectively

Received Feb. 20, 1985; presented as Paper 85-0585 at the AIAA/ASME/ASCE/AHS 26th Structures, Structural Dynamics and Materials Conference, April 15-17, 1985; revision received Dec. 4, 1985.

*Research Scientist, Unsteady Aerodynamics Branch, Loads and Aeroelasticity Division. Member AIAA.

Introduction

COMPUTATIONAL methods employing linear theory have been developed for the prediction of unsteady flowfields about aerodynamically interfering lifting surfaces.[1,2] These methods are extensions of linearized theory for single lifting surfaces to more complicated configurations such as two lifting surfaces in tandem. Applications of these methods are restricted to subsonic or supersonic flows because of the underlying linear theories on which they are based. In the transonic regime, computational methods for modeling flowfields about oscillating multiple lifting surface configurations have yet to be developed.

Steady transonic flowfields and interference effects about two-dimensional canard-wing systems have been studied by Shankar et al.[3] Using transonic small-disturbance theory, the interference flowfields were computed in preparation for solving the three-dimensional interaction problem. In Ref. 3, a double grid arrangement was used whereby the canard and wing were placed in separate computational domains. Results showed a favorable increase in overall lift established by appropriate placement of the canard and wing. Steady transonic computational results for three-dimensional canard-wing configurations, including comparisons with experimental data, have been reported in Refs. 4 and 5. Shankar and Malmuth[4] presented computations for a few canard-wing configurations obtained by placing the two surfaces in a sheared fine-grid system embedded in a global Cartesian crude grid. A weakening of the wing shock due to the canard downwash was illustrated by Mach number contour plots. Shankar and Goebel[5] developed a local numerical mapping procedure where the leading and trailing edges of the two surfaces are treated as constant coordinate lines in the computational domain. Computed results for a closely coupled canard-wing research model were in good agreement with experimental data. Also in Ref. 5, inaccuracies were demonstrated in results computed using double grid arrangements for closely coupled canard-wing systems.

The purpose of this paper is to present unsteady transonic results for two-dimensional canard-wing configurations as a first step toward solving the unsteady three-dimensional in-

teraction problem. The objectives of the study were to 1) develop an unsteady transonic computational capability for aerodynamically interfering airfoils, 2) investigate the effects of two-dimensional canard-wing aerodynamic interference on transonic steady pressures and unsteady forces, and 3) determine the effects of canard-wing separation distance on transonic unsteady airloads, aeroelastic stability, and flutter, for a limited number of configurations. In this study, the aerodynamic calculations were performed by extending the XTRAN2L[6] transonic small-disturbance code to allow the treatment of an additional airfoil. The computational developments presented herein helped to identify problems that may be encountered in developing the three-dimensional capability. The study further provides a relatively inexpensive examination of the unsteady transonic interactions between oscillating airfoils. The leading airfoil has been termed the "canard," and the trailing airfoil the "wing." Steady transonic pressure distributions and Mach number contour plots are presented for isolated airfoil and canard-wing configurations. Unsteady transonic forces due to plunge and pitch motions of the canard and wing are shown. Results for a variety of canard-wing separation distances were obtained to determine the effects of aerodynamic interference on unsteady transonic airloads. These transonic airloads are used in aeroelastic analyses to demonstrate the application of the XTRAN2L canard-wing computational capability and to investigate the effects of aerodynamic interference on aeroelastic stability and flutter.

Computational Procedures

Transonic Code XTRAN2L

The original LTRAN2 code of Ballhaus and Goorjian[7] was developed to time-accurately integrate the low-frequency transonic small-disturbance (TSD) equation with steady-state airfoil and wake boundary conditions. Houwink and Van der Vooren[8] extended the range of usable frequencies by adding the time-derivative terms to the airfoil and wake boundary conditions. The resulting code was termed LTRAN2-NLR. The XTRAN2L code is an extensive modification of LTRAN2-NLR which was developed at the NASA Langley Research Center. The program solves the complete TSD equation and includes monotone differencing, nonreflecting farfield boundary conditions, an improved grid, a pulse transient capability, and time-marching aeroelastic analyses. Details of the XTRAN2L algorithm development and modifications are given by Whitlow.[6] Details of the grid development and pulse capability are given by Seidel et al.[9]

Two-dimensional canard-wing calculations were performed by extending the alternating-direction implicit (ADI) solution procedure of XTRAN2L to include an additional airfoil. The program is now capable of computing unsteady transonic flowfields about relatively general interfering airfoil configurations. The present program coding, however, does not allow for overlapping or coplanar configurations.

The two-dimensional canard-wing geometry considered is shown in Fig. 1a. Horizontal separation distance is defined in units of wing chord from wing midchord to canard midchord by S; vertical separation distance is defined in units of wing chord by D. The XTRAN2L grid near the canard-wing system is shown in Fig. 1b. Flat horizontal wakes are assumed for both canard and wing. The grid is based on the XTRAN2L default grid described in Ref. 9 and, for the configuration shown ($S=1.0$, $D=0.25$), has 116 and 66 points in the horizontal and vertical directions, respectively. In the streamwise direction, 30 and 50 equidistantly spaced points are distributed along the canard and wing, respectively. One additional point is added near the leading edge of each airfoil for better resolution. Grid stretching to the farfield is identical to that described in Ref. 9. For example, upstream of the canard and downstream of the wing, gridpoints are stretched 20 wing chordlengths to the farfield boundaries. Above the canard and below the wing, gridpoints are stretched 25 wing chordlengths to the farfield boundaries. Between the two airfoils, vertical gridlines are distributed equidistantly between the first gridpoint downstream of the canard trailing edge and the wing leading edge. Horizontal gridlines are distributed equidistantly between the airfoil centerlines with one additional line placed symmetrically below the canard centerline and another additional line placed symmetrically above the wing centerline. For different canard-wing separation distances, points are added or removed to maintain similar grid spacing.

Pulse Transfer-Function Analysis

Unsteady aerodynamic forces are computed for two modes of airfoil motion: pitch about the quarter-chord and vertical translation (plunge). Typically, unsteady aerodynamic forces are determined by calculating several cycles of forced harmonic oscillation with the last cycle providing the estimate of the forces. Alternatively, harmonic forces may be obtained indirectly from the response due to a smoothly varying exponentially shaped pulse.[9] In this procedure, the airfoil is given a small prescribed pulse in a given mode of motion (either plunge or pitch) and the aerodynamic transients calculated. For pitch motion, the input pulse is given by

$$\alpha=\alpha_0+\alpha_1\exp[-0.25(\tau-17.5\Delta\tau)^2] \quad (1)$$

and for plunge motion, the input pulse is given by

$$h=h_1\exp[-0.25(\tau-17.5\Delta\tau)^2] \quad (2)$$

where $\Delta\tau$ is the nondimensional time step. The harmonic response is obtained by a transfer-function analysis using fast Fourier transforms (FFT). Use of the pulse transfer-function technique gives considerable detail in the frequency domain with a significant reduction in cost over the alternative method of calculating multiple oscillatory responses.

Pulse transient calculations were performed using 1024 time steps with $\Delta\tau$ set equal to $5\pi/32$. Plunge pulse and pitch pulse

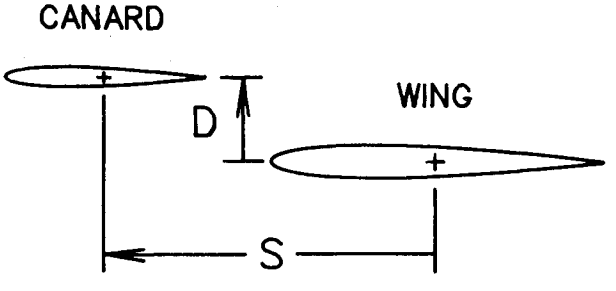

a) Two-dimensional canard-wing geometry.

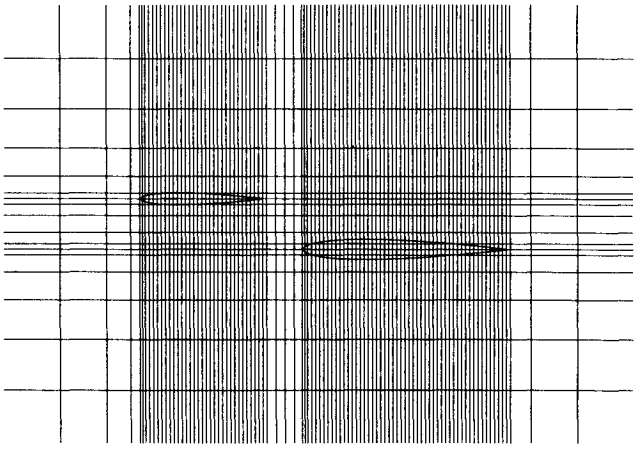

b) XTRAN2L grid near canard-wing system.

Fig. 1 Geometry definition and finite difference grid.

amplitudes were $h_1 = 0.01$ and $\alpha_1 = 0.1$ deg, respectively, for both canard and wing.

Aeroelastic Model

For aeroelastic analysis, the wing was assumed to have plunge and pitch degrees of freedom and the canard was assumed to be motionless. Thus the canard influences the stability of the wing through aerodynamic coupling only. The structural equations of motion used for the wing are the classical equations for an airfoil section oscillating with plunge and pitch motions.[10] Aeroelastic parameter values selected were $a = -0.5$, $x_\alpha = 0.2$, $r_\alpha = 0.5$, $\omega_h/\omega_\alpha = 0.3$, and $\mu = 60$.

Aeroelastic stability calculations were performed using a state-space aeroelastic model termed the Padé model.[11,12] This model is formulated by curve-fitting the unsteady aerodynamic forces by a Padé approximating function.[11] These approximating functions are then expressed as linear differential equations which, when coupled to the structural equations of motion, lead to the first-order matrix equation

$$\{\dot{Z}\} = [A]\{Z\} \tag{3}$$

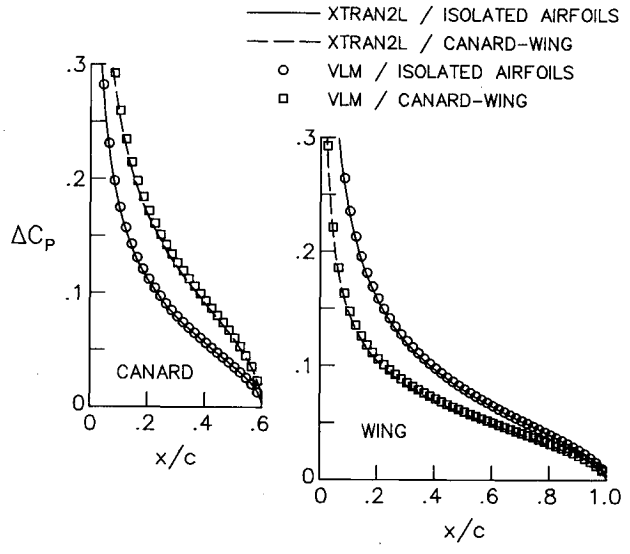

Fig. 2 Comparison of lifting pressure coefficients computed using XTRAN2L and a vortex-lattice method (VLM) for flat plates at $M = 0.5$ and $\alpha_0 = 1.0$ deg ($S = 1.0$, $D = 0.25$).

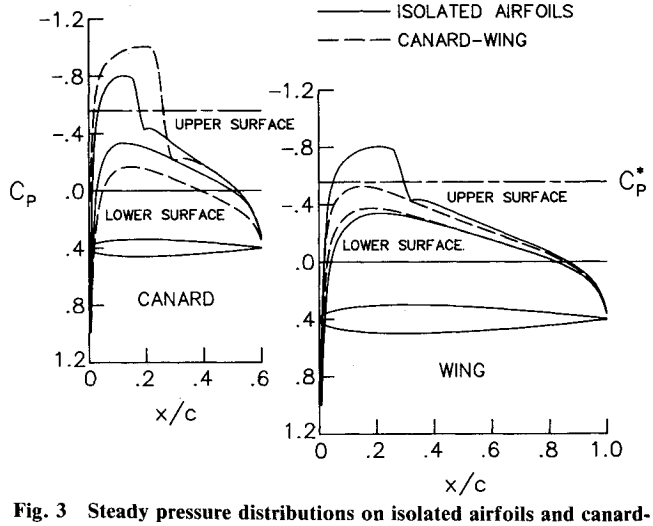

Fig. 3 Steady pressure distributions on isolated airfoils and canard-wing ($S = 1.0$, $D = 0.25$) NACA 0010 configurations at $M = 0.76$ and $\alpha_0 = 1.0$ deg.

where $\{Z\}$ is a state vector containing displacements, velocities, and augmented states. The augmented states model the unsteady airloads. Stability analyses are performed by a linear eigenvalue solution of the Padé model. Real and imaginary parts of the eigenvalues (damping and frequency, respectively) are plotted in a dynamic pressure "root-locus" type format in the complex s plane.

Results and Discussion

Steady pressure calculations for a simple case of two flat-plate airfoils were performed first to assess the XTRAN2L code modifications by comparison with an independent vortex-lattice method (VLM) program. The freestream Mach number was $M = 0.5$; the mean angle of attack was $\alpha_0 = 1.0$ deg for both airfoils; the canard chordlength was selected to be 60% of the wing chordlength; and the horizontal and vertical separation distances were $S = 1.0$ and $D = 0.25$, respectively. The lifting pressure coefficient, ΔC_p, is plotted in Fig. 2 for isolated airfoils and closely coupled canard-wing configurations. The XTRAN2L results are in excellent agreement with the results from the VLM program. As shown in Fig. 2, the area between the isolated airfoil ΔC_p curves and the canard-wing ΔC_p curves represents the steady aerodynamic interference between the two airfoils. For the configuration shown, the canard induces a downwash on the wing, thus decreasing its ΔC_p and lift. Conversely, the wing induces an upwash on the canard that increases its ΔC_p and lift.

For transonic XTRAN2L computations, the NACA 0010[13] airfoil section was selected for both canard and wing. The freestream Mach number was set equal to 0.76, and the canard chordlength was selected to be 60% of the wing chordlength. Results were obtained only for $\alpha_0 = 1.0$ deg since the in-

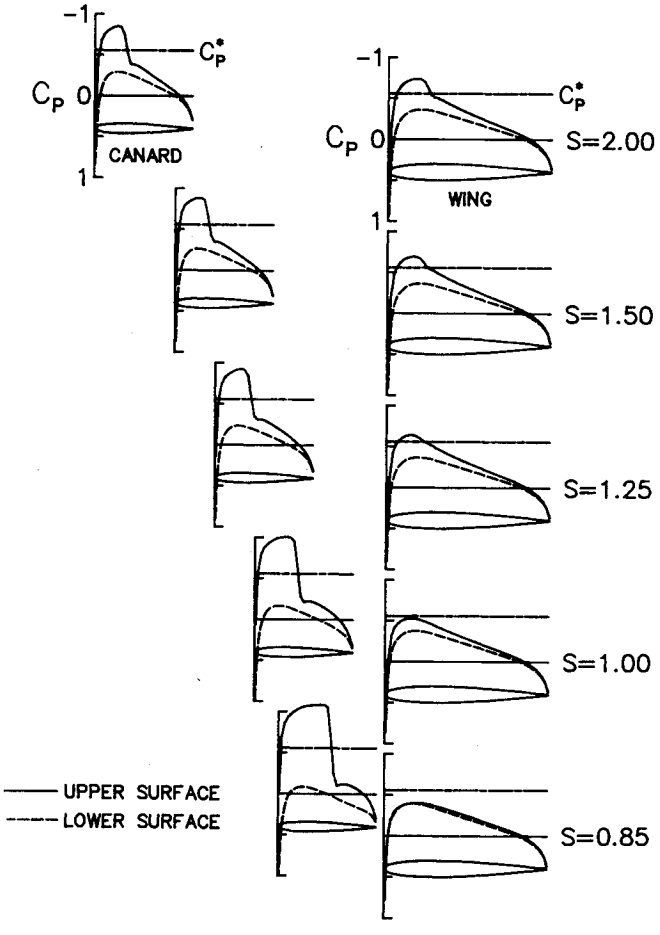

Fig. 4 Steady pressure distributions on NACA 0010 canard-wing for a range of horizontal separation distance S ($D = 0.25$) at $M = 0.76$ and $\alpha_0 = 1.0$ deg.

terference effects for different values of mean angle of attack were not expected to be significantly different in character than the effects for $\alpha_0 = 1.0$ deg. Canard-wing horizontal and vertical separation distances were $S = 1.0$ and $D = 0.25$, respectively, except where otherwise noted. These cases were selected to demonstrate the new unsteady transonic capability for aerodynamically interfering airfoil configurations. The author is unaware of any experimental data for interfering airfoils that could be used for code validation purposes. Comparisons with steady and unsteady experimental data have been reported in Refs. 14 and 15, though, for isolated airfoil cases using XTRAN2L. Since the present work involves a modification to the XTRAN2L code, it is expected that the interfering airfoil version should give an accuracy similar to the original single airfoil code.

Steady Transonic Interference

Steady pressure distributions for the isolated airfoil are shown by the solid lines in Fig. 3. A shock wave of moderate strength is present on the upper surfaces near 30% chord; the lower surfaces are entirely subcritical. Steady pressure distributions on the closely coupled canard-wing configuration are also shown in Fig. 3 (dashed lines). For this configuration the canard produces a downwash on the wing that eliminates the shock such that the flow about the wing is entirely subcritical. Conversely, the wing produces an upwash on the canard such that the canard upper surface shock is increased in strength and located further aft near 44% chord.

Transonic steady pressure distributions for a range of horizontal and vertical separation distances were obtained. Results for horizontal separation $S = 0.85$, 1.0, 1.25, 1.5, and 2.0, with constant vertical separation $D = 0.25$, are shown in Fig. 4. As the distance between the canard and wing becomes small, the shock on the canard upper surface increases in strength. The shock on the upper surface of the wing decreases in strength and then disappears, with decreasing horizontal separation distance. Results for a range of vertical separation distance show very similar steady transonic interference effects and, therefore, are not shown here.

Mach number contour lines for the isolated airfoils and several canard-wing configurations are shown in Fig. 5. The Mach contour interval is $\Delta M = 0.04$. For the isolated airfoils (Fig. 5a), the shock wave is represented by the close proximity of contour lines on the upper surfaces near 30% chord. For the canard-wing configurations (Figs. 5b-d), the contour lines along the wing's upper surface become relatively evenly spaced with the weakening and disappearance of the shock. The contour lines along the canard's upper surface indicate the presence of a strong shock wave especially for the closely coupled configuration with $S = 1.0$ and $D = 0.25$ (Fig. 5d). These Mach number contours further illustrate the steady transonic interaction between the two airfoils by the contour lines that form between the canard and wing with decreasing separation distance.

Unsteady Transonic Interference

The effects of aerodynamic interference on unsteady pressure distributions are similar to the effects on steady pressures (shown in Figs. 2-4) and, therefore, are not shown here. Instead, these effects are demonstrated on unsteady airloads which can then be shown for a wide range of reduced frequency which is in contrast with showing the effects on unsteady pressures at only one or two values of reduced frequency. The unsteady transonic airloads were computed using the pulse transfer-function analysis method. Sample time histories for an input wing pitch pulse and the resulting wing and canard lift coefficients are shown in Fig. 6. Only the first 102 time steps are plotted. (Moment coefficient time histories are also computed for both canard and wing but are not shown here.) The aerodynamic forces in the frequency domain are determined by dividing the FFT of the output lift coeffi-

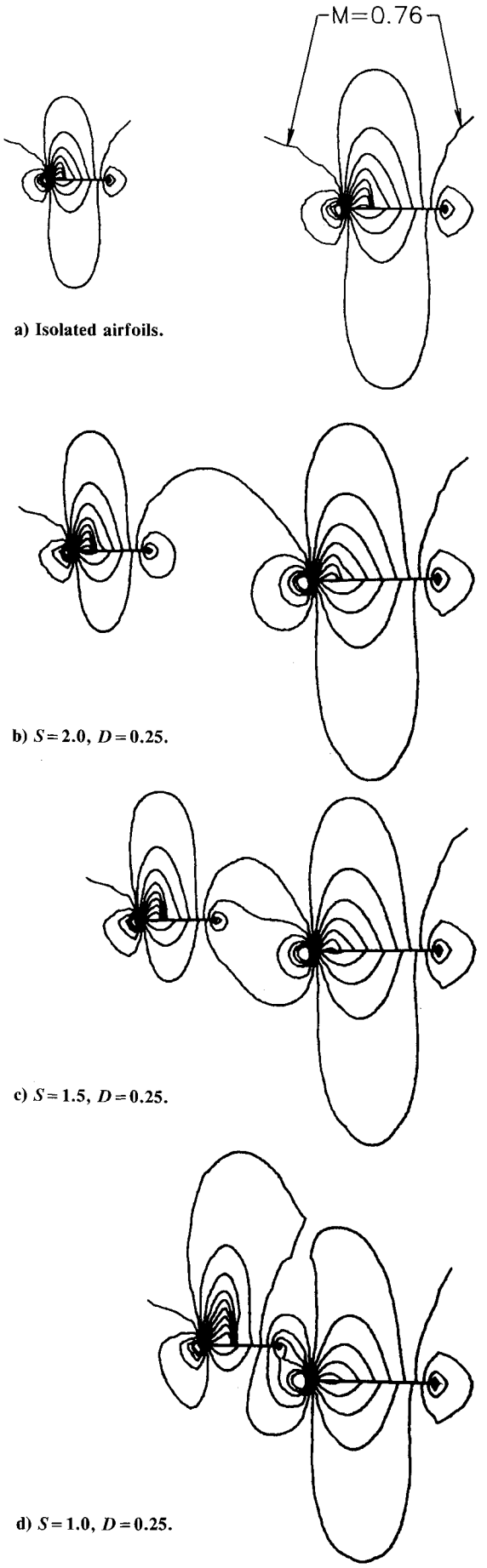

a) Isolated airfoils.

b) $S = 2.0$, $D = 0.25$.

c) $S = 1.5$, $D = 0.25$.

d) $S = 1.0$, $D = 0.25$.

Fig. 5 Mach number contour lines ($\Delta M = 0.04$) for isolated and various NACA 0010 canard-wing configurations at $M = 0.76$ and $\alpha_0 = 1.0$ deg.

cient time histories by the FFT of the input wing pitch pulse. The resulting wing lift coefficient due to wing pitch and canard lift coefficient due to wing pitch are shown in Figs. 7a and 7b, respectively. These coefficients are plotted as real and imaginary functions of reduced frequency k. (The unsteady aerodynamic coefficients Q_{ij} are defined as listed in Table 1.) To assess the applicability of the pulse transfer-function analysis to two-dimensional canard-wing configurations, harmonic oscillatory solutions were obtained for discrete values of reduced frequency. Unsteady wing and canard lift coefficients due to wing pitch, computed by the pulse transfer-function analysis, are compared with coefficients from the oscillatory analysis in Fig. 7. The close agreement between pulse and oscillatory forces thus verifies the extension of the pulse analysis to canard-wing geometries and demonstrates the ability of the pulse analysis to accurately predict transonic unsteady aerodynamic interference effects.

Self-induced unsteady airloads on the canard and wing due to motion of the respective airfoils, computed using the pulse transfer-function analysis, are presented in Figs. 8 and 9. These unsteady airloads are compared with the isolated airfoil airloads to demonstrate the effects of aerodynamic interference. Wing lift and moment coefficients due to wing plunge are shown in Figs. 8a and 8b, respectively; wing lift and moment coefficients due to wing pitch are shown in Figs. 8c and 8d, respectively. In general, the wing forces due to wing plunge motion show only small differences between isolated airfoil and canard-wing cases. However, large differences between the two sets of results occur in the real and imaginary parts of the wing lift coefficient due to wing pitch (Fig. 8c), for low values of reduced frequency k. The magnitudes of the real and imaginary parts for low k values are significantly reduced for the canard-wing configuration because the mean flow about the wing is entirely subcritical due to the presence of the canard. This is evident from the steady pressure distributions on the wing as shown in Fig. 3. Similar comparisons of self-induced unsteady airloads on the canard are shown in Fig. 9. Canard lift and moment coefficients due to canard plunge are shown in Figs. 9a and 9b, respectively; canard lift and moment coefficients due to canard pitch are shown in Figs. 9c and 9d, respectively. For the canard airloads due to canard motion,

Table 1 Definition of unsteady aerodynamic coefficient Q_{ij}

i	j	Unsteady coefficient	Due to motion
1	1	Wing lift	Wing plunge
1	2	Wing lift	Wing pitch
1	3	Wing lift	Canard plunge
1	4	Wing lift	Canard pitch
2	1	Wing moment	Wing plunge
2	2	Wing moment	Wing pitch
2	3	Wing moment	Canard plunge
2	4	Wing moment	Canard pitch
3	1	Canard lift	Wing plunge
3	2	Canard lift	Wing pitch
3	3	Canard lift	Canard plunge
3	4	Canard lift	Canard pitch
4	1	Canard moment	Wing plunge
4	2	Canard moment	Wing pitch
4	3	Canard moment	Canard plunge
4	4	Canard moment	Canard pitch

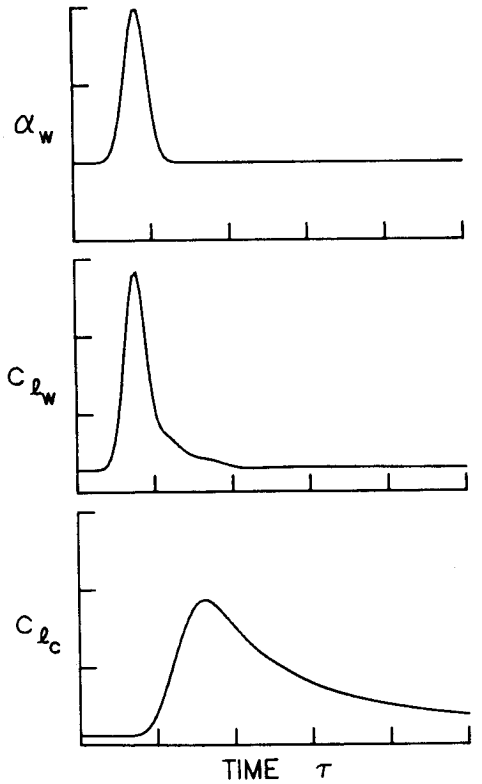

Fig. 6 Wing pitch pulse and resulting wing and canard lift coefficient time histories for a closely coupled ($S=1.0$, $D=0.25$) NACA 0010 canard-wing at $M=0.76$ and $\alpha_0=1.0$ deg.

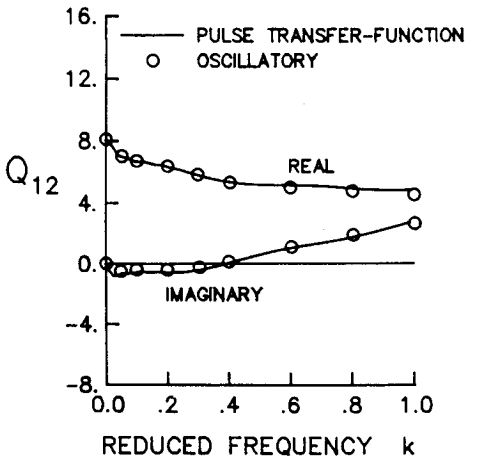

a) Wing lift coefficient due to wing pitch.

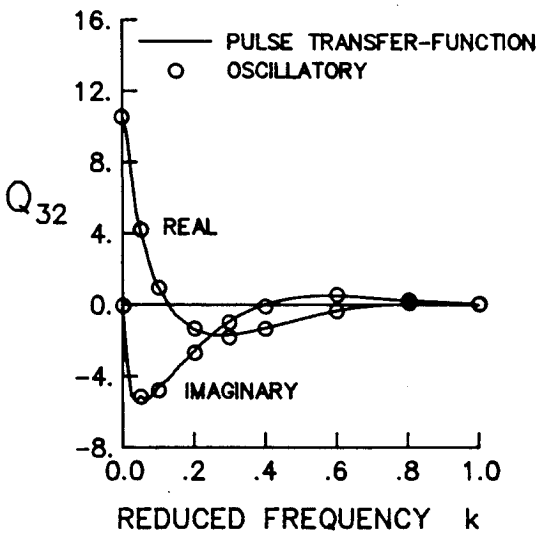

b) Canard lift coefficient due to wing pitch.

Fig. 7 Comparison between unsteady lift coefficients calculated by pulse analysis with oscillatory analysis for a closely coupled ($S=1.0$, $D=0.25$) NACA 0010 canard-wing at $M=0.76$ and $\alpha_0=1.0$ deg.

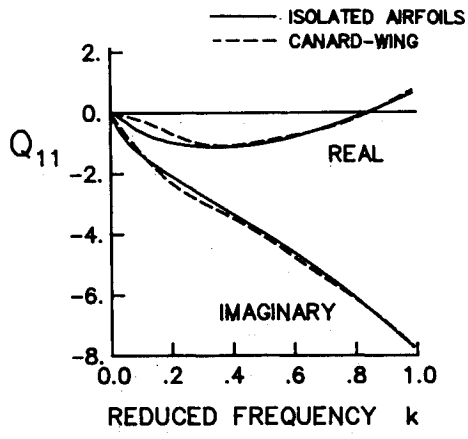

a) Wing lift coefficient due to wing plunge.

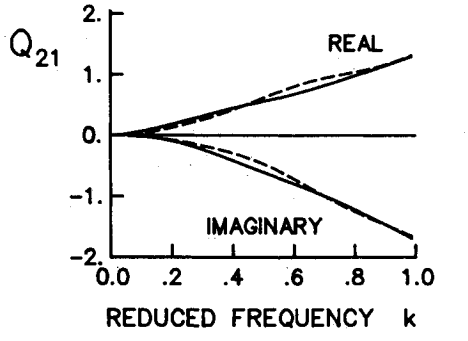

b) Wing moment coefficient due to wing plunge.

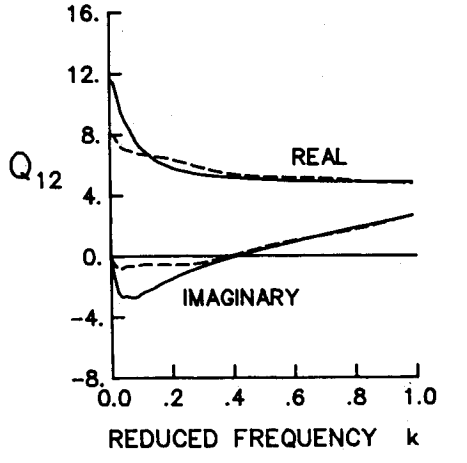

c) Wing lift coefficient due to wing pitch.

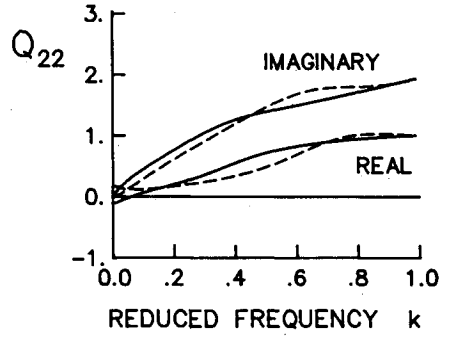

d) Wing moment coefficient due to wing pitch.

Fig. 8 Unsteady wing coefficients for isolated airfoil and canard-wing ($S=1.0$, $D=0.25$) NACA 0010 configurations at $M=0.76$ and $\alpha_0=1.0$ deg.

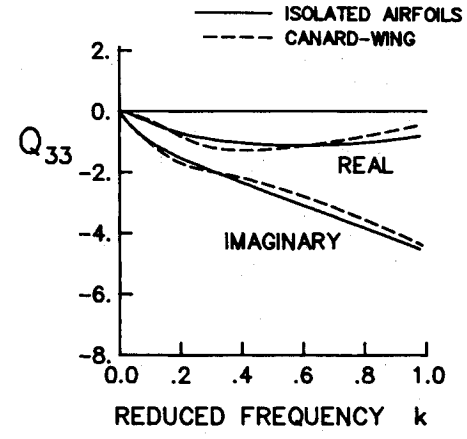

a) Canard lift coefficient due to canard plunge.

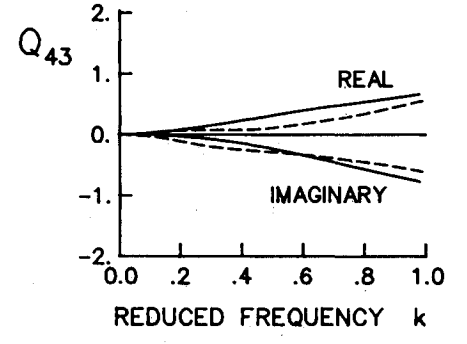

b) Canard moment coefficient due to canard plunge.

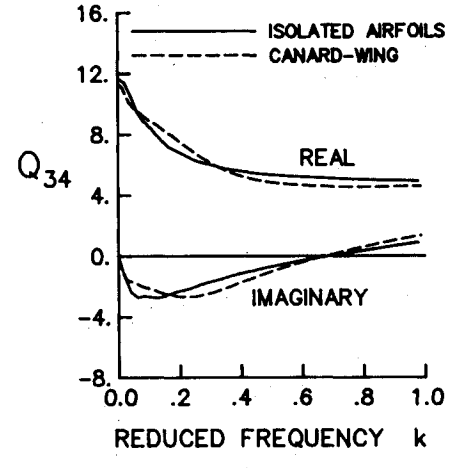

c) Canard lift coefficient due to canard pitch.

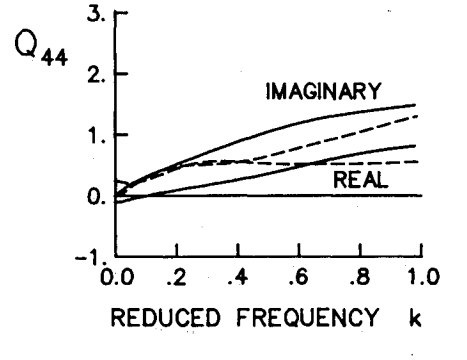

d) Canard moment coefficient due to canard pitch.

Fig. 9 Unsteady canard coefficients for isolated airfoil and canard-wing ($S=1.0$, $D=0.25$) NACA 0010 configurations at $M=0.76$ and $\alpha_0=1.0$ deg.

the differences between isolated airfoil and canard-wing results are generally small, except for the canard moment coefficient due to canard pitch (Fig. 9d).

Oscillatory motion of the wing induces harmonic lift and moment on the fixed canard. Conversely, unsteady motion of the canard induces unsteady lift and moment on the fixed wing. Examples of these induced unsteady transonic airloads as functions of reduced frequency are shown in Figs. 10 and 11. Results were obtained for a variety of horizontal and vertical separation distances, although unsteady forces are plotted here for $S = 0.85$, 1.0, 1.25, 1.5, and 2.0, with $D = 0.25$ only. Figures 10a and 10b show the canard lift coefficient due to wing plunge and the canard lift coefficient due to wing pitch, respectively. In both cases, the induced unsteady airloads become considerably larger when the separation distance becomes smaller, as expected. Real and imaginary parts of the unsteady airloads, for a given separation distance S, are very similar in shape in comparison with those at other values of S, when the reduced frequency axis is either stretched or compressed. As shown in Fig. 10a, for example, the first zero-crossing of the real part of Q_{31} occurs at successively increasing values of k for a monotonically decreasing separation distance S. This trend is physically related to the shorter time required for disturbances created by the wing to influence the canard as the separation distance is decreased. The forces are also largest at low values of reduced frequency and tend to decrease in magnitude at higher values of reduced frequency. The large magnitudes at low reduced frequency are qualitatively consistent with the relatively long times associated with upstream-propagating disturbances (from wing to canard) in comparison with downstream-propagating disturbances (from canard to wing).

Figures 11a and 11b show the wing lift coefficients due to canard plunge and canard pitch, respectively. In contrast with the results of Fig. 10, these induced unsteady airloads do not tend to zero as the horizontal separation distance S becomes large. This is because the oscillatory wake of the canard is in close proximity ($D = 0.25$) above the wing which influences

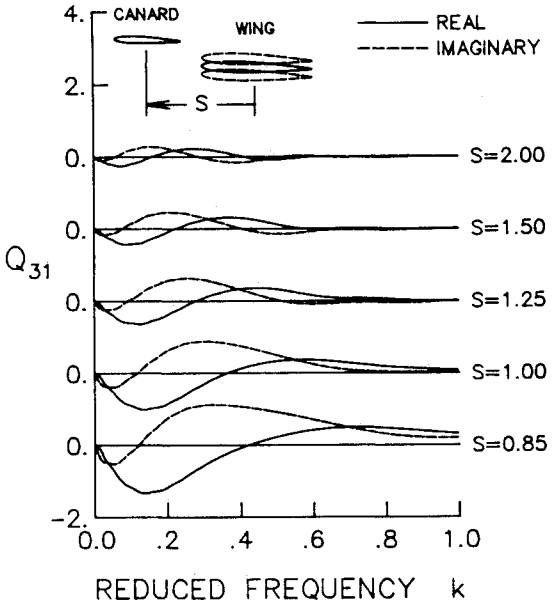

a) Canard lift coefficient due to wing plunge.

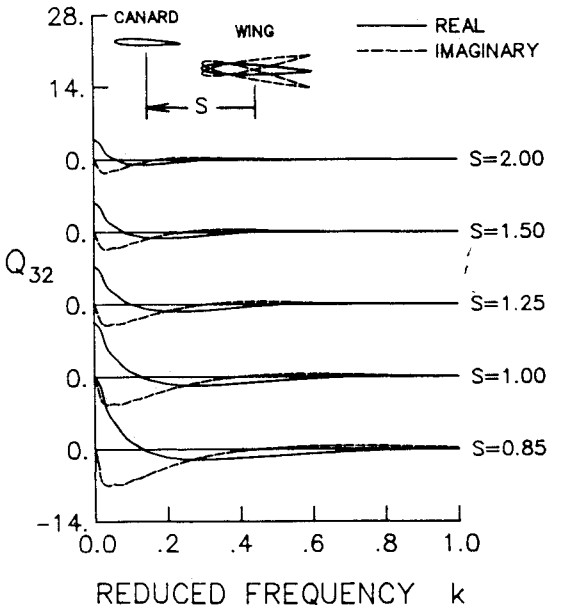

b) Canard lift coefficient due to wing pitch.

Fig. 10 Unsteady canard lift coefficients induced by wing motion for a range of horizontal separation distance S at $M = 0.76$ and $\alpha_0 = 1.0$ deg ($D = 0.25$).

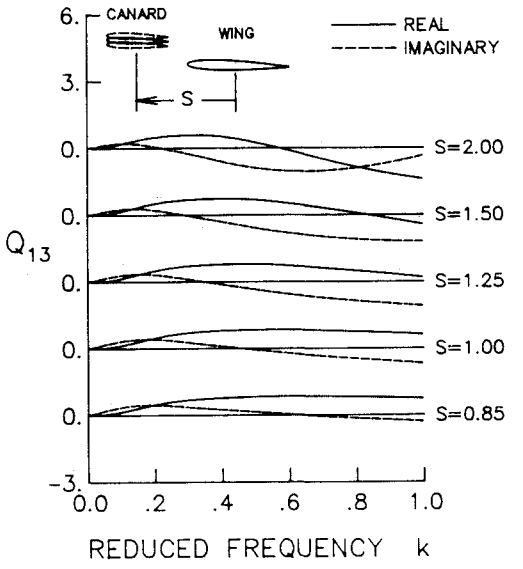

a) Wing lift coefficient due to canard plunge.

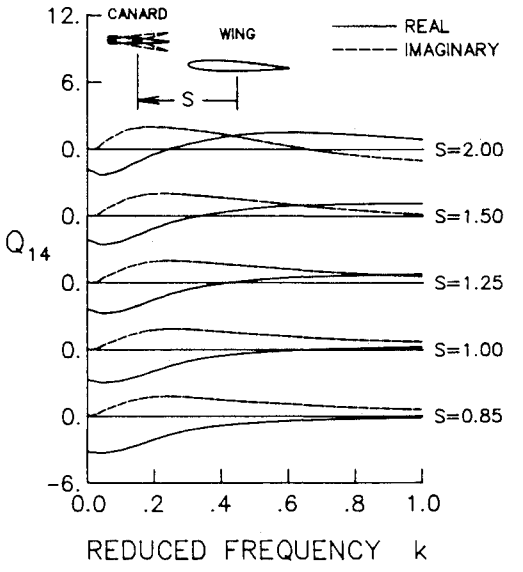

b) Wing lift coefficient due to canard pitch.

Fig. 11 Unsteady wing lift coefficients induced by canard motion for a range of horizontal separation distance S at $M = 0.76$ and $\alpha_0 = 1.0$ deg ($D = 0.25$).

wing pressures and, hence, wing lift, even for large values of S. Also in contrast with the results of Fig. 10, the induced airloads of Fig. 11 are of sizeable magnitude at the higher values of reduced frequency. This characteristic is attributed to the relatively shorter times for disturbances to propagate downstream from the oscillating canard to the motionless wing in comparison with upstream propagation from wing to canard.

Aeroelastic Applications

To investigate the effects of aerodynamic interference on aeroelastic stability and flutter, Padé model stability calculations were performed. Dynamic pressure root-loci of the wing for isolated airfoil and closely coupled canard-wing configurations are shown in Fig. 12. With increasing flight dynamic pressure $\bar{q}$, the wing pitch mode moves to the left in the stable left half of the complex s-plane. The plunge-dominated root-locus becomes the flutter mode at dynamic pressures of $\bar{q}_F = 0.21$ and 0.35 for the isolated airfoil and closely coupled canard-wing configurations, respectively. For the case considered, inclusion of the motionless canard in the transonic flowfield lowers the wing pitch modal frequency and increases damping in the wing plunge mode, thus delaying the onset of flutter. A 67% increase in flutter dynamic pressure $\bar{q}_F$ (or equivalently, a 29% increase in flutter speed index V_F) was obtained with the inclusion of the canard. The increase in wing flutter speed for the closely coupled configuration is attributed to decreased transonic effects on the wing caused by the canard downwash. Flutter speeds for a range of canard-wing horizontal and vertical separation are plotted in Fig. 13. As the separation distance between the aeroelastic wing and the aerodynamically interfering canard decreases, the wing flutter speed increases. The flutter speed index V_F vs vertical separation distance D curve shown in Fig. 13 is not symmetric about the $D=0$ line because the two airfoils are at 1 deg mean angle of attack. The flutter results would be symmetric about $D=0$ if the airfoils were at 0-deg mean angle of attack.

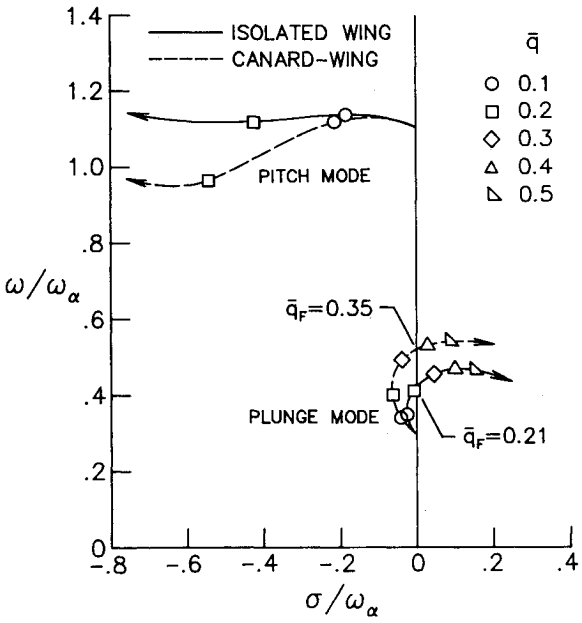

Fig. 12 Wing dynamic pressure root-loci for isolated airfoil and canard-wing ($S=1.0$, $D=0.25$) NACA 0010 configurations at $M=0.76$ and $\alpha_0=1.0$ deg.

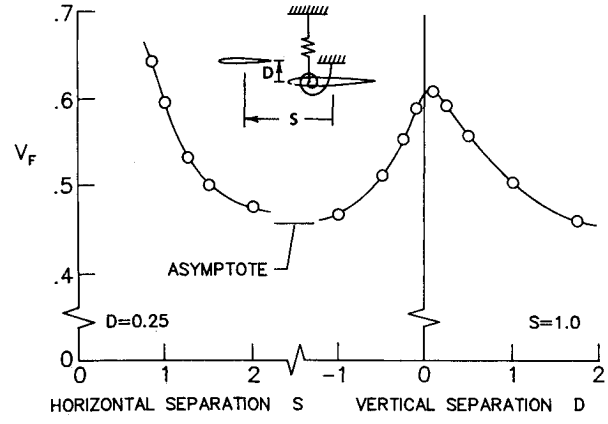

Fig. 13 Flutter boundaries for canard-wing horizontal and vertical separation distances at $M=0.76$ and $\alpha_0=1.0$ deg.

Concluding Remarks

Unsteady transonic flow calculations for aerodynamically interfering airfoil configurations have been performed as a first step toward solving the three-dimensional canard-wing interaction problem. These calculations were performed by extending the XTRAN2L unsteady transonic small-disturbance code to include an additional airfoil. The code is now capable of computing unsteady transonic flowfields about relatively general two-dimensional canard-wing geometries. The results presented using this new computational capability provided a relatively inexpensive examination of the unsteady transonic interactions between oscillating airfoils.

For the configurations studied, the canard produced a downwash field on the wing that weakened or eliminated the wing shock. Conversely, the wing produced an upwash field on the canard that increased the canard shock strength. Mach number contour lines for several canard-wing configurations clearly illustrated the steady transonic interaction between the two airfoils. Unsteady transonic airloads as a function of reduced frequency were computed by extending a pulse transfer-function analysis to canard-wing configurations. The accuracy of this analysis was confirmed by the excellent agreement found between unsteady airloads computed by pulse analysis and those calculated by oscillatory analysis. Results for a range of canard-wing horizontal separation distance revealed the effects of aerodynamic interference on transonic unsteady airloads. Aeroelastic analyses employing these unsteady airloads demonstrated the effects of aerodynamic interference on aeroelastic stability and flutter. Inclusion of the canard in the transonic flowfield lowered the wing pitch modal frequency and increased damping in the wing plunge mode, thus delaying the onset of flutter. With decreased canard-wing separation distance, beneficial increases in wing flutter speed resulted due to the aerodynamically interfering canard.

References

[1] *Proceedings of the AGARD Symposium on Unsteady Aerodynamics for Aeroelastic Analyses of Interfering Surfaces,* Tonsberg, Norway, AGARD-CP-80-71, April 1971.

[2] Rodden, W. P., "A Comparison of Methods Used in Interfering Lifting Surface Theory," AGARD Rept. 643, Feb. 1976.

[3] Shankar, V., Malmuth, N. D., and Cole, J. D., "Transonic Flow Calculations over Two-Dimensional Canard-Wing Systems," *Journal of Aircraft,* Vol. 18, Feb. 1981, pp. 108-114.

[4] Shankar, V. and Malmuth, N. D., "Computational Treatment of Transonic Canard-Wing Interactions," AIAA Paper 82-0161, Jan. 1982.

[5] Shankar, V. and Goebel, T., "A Numerical Transformation Solution Procedure for Closely Coupled Canard-Wing Transonic Flows," AIAA Paper 83-0502, Jan. 1983.

[6] Whitlow, W. Jr., "XTRAN2L: A Program for Solving the General Frequency Unsteady Transonic Small Disturbance Equation," NASA TM 85723, Nov. 1983.

[7] Ballhaus, W. F. and Goorjian, P. M., "Implicit Finite-Difference

Computations of Unsteady Transonic Flows about Airfoils," *AIAA Journal,* Vol. 15, Dec. 1977, pp. 1728-1735.

[8]Houwink, R. and Van der Vooren, J., "Improved Version of LTRAN2 for Unsteady Transonic Flow Computations," *AIAA Journal,* Vol. 18, Aug. 1980, pp. 1008-1010.

[9]Seidel, D. A., Bennett, R. M., and Whitlow, W. Jr., "An Exploratory Study of Finite Difference Grids for Transonic Unsteady Aerodynamics," NASA TM 84583, Dec. 1982.

[10]Bisplinghoff, R. L., Ashley, H., and Halfman, R. L., *Aeroelasticity,* Addison-Wesley, Reading, MA, 1955.

[11]Batina, J. T. and Yang, T. Y., "Application of Transonic Codes to Aeroelastic Modeling of Airfoils Including Active Controls," *Journal of Aircraft,* Vol. 21, Aug. 1984, pp. 623-630.

[12]Batina, J. T. and Yang, T. Y., "Transonic Time-Responses of the MBB A-3 Supercritical Airfoil Including Active Controls," *Journal of Aircraft,* Vol. 22, May 1985, pp. 393-400.

[13]Abbott, I. H. and Von Doenhoff, A. E., *Theory of Wing Sections,* Dover Pub., New York, 1959.

[14]Bland, S. R. and Seidel, D. A., "Calculation of Unsteady Aerodynamics for Four AGARD Standard Aeroelastic Configurations," NASA TM 85817, May 1984.

[15]Edwards, J. W., Bland, S. R., and Seidel, D. A., "Experience with Transonic Unsteady Aerodynamic Calculations," AGARD-CP-374, Jan. 1985, pp. 5-1 to 5-21; also, NASA TM 86278, Aug. 1984.